Simulation-Based Prediction of Phosphatidylinositol 4,5-Bisphosphate Binding to an Ion Channel

Matthias R. Schmidt,[†] Phillip J. Stansfeld,[†] Stephen J. Tucker,[‡] and Mark S. P. Sansom*,[†]

[†]Department of Biochemistry, University of Oxford, Oxford OX1 3QU, United Kingdom
[‡]Clarendon Laboratory, Department of Physics, University of Oxford, Oxford OX1 3PU, United Kingdom

ⓢ *Supporting Information*

ABSTRACT: Protein−lipid interactions regulate many membrane protein functions. Using a multiscale approach that combines coarse-grained and atomistic molecular dynamics simulations, we have predicted the binding site for the anionic phospholipid phosphatidylinositol 4,5-bisphosphate (PIP_2) on the Kir2.2 inwardly rectifying (Kir) potassium channel. Comparison of the predicted binding site to that observed in the recent PIP_2-bound crystal structure of Kir2.2 reveals good agreement between simulation and experiment. In addition to providing insight into the mechanism by which PIP_2 binds to Kir2.2, these results help to establish the validity of this multiscale simulation approach and its future application in the examination of novel membrane protein−lipid interactions in the increasing number of high-resolution membrane protein structures that are now available.

Interactions of lipids with membrane proteins are an important component of many cell signaling pathways. The anionic lipid phosphatidylinositol 4,5-bisphosphate (PIP_2) plays a major role in such processes by acting as a secondary messenger, localizing proteins to membranes, and regulating the activity of many different classes of ion channels.[1] One of the effects of PIP_2 is the direct activation of inwardly rectifying (Kir) potassium channels that modulate cellular electrical activity, and whose dysfunction underlies a wide range of inherited channelopathies.[2,3] The binding site for PIP_2 in Kir channels was previously predicted using both conventional docking methods and simulation-based approaches.[4−6] However, these previous studies all employed homology models based upon the structure of a chimera between a eukaryotic and prokaryotic Kir channel in which several of the residues proposed to interact with PIP_2 were not fully resolved [Protein Data Bank (PDB) entry 2QKS]. Furthermore, this chimeric Kir/KirBac channel exhibits a complex functional interaction with PIP_2, and it is known that PIP_2 inhibits prokaryotic Kir channels.[7,8] Consequently, the accuracy of the binding site predicted in these original simulations remains uncertain.

In this study, we have now taken advantage of several recently determined X-ray crystal structures of eukaryotic Kir channels to evaluate the binding site for PIP_2 in the Kir2.2 channel using a multiscale molecular dynamics simulation approach.[5] This method employed coarse-grained (CG) simulations to predict initial PIP_2 binding events that were then refined by subsequent atomistic (AT) simulations.[9−13] To

validate this prediction, the simulations were then compared to the crystal structures of Kir2.2 with either PIP_2 (PDB entry 3SPI) or the anionic lipid phosphatidic acid (PPA) bound (PDB entry 3SPC). An apo-state structure without any bound lipid has also been determined (PDB entry 3JYC),[14,15] and these different structures suggest an activation mechanism in which PIP_2 binding induces an upward translation and engagement of the C-terminal domain (CTD) with the transmembrane domain (TMD).[14]

To explore the influence of these different initial conformations on these predictions as well as possible effects of the lipid bilayer, bound phospholipids were removed from the 3SPI and 3SPC Kir2.2 structures, and both structures were then used as input for multiscale simulations of PIP_2 binding (Figure 1). To assess binding of PIP_2 to a Kir2.2 apo state, we also performed CG simulations using the 3JYC structure as input (Figure S1 of the Supporting Information). In addition to comparing our predicted binding sites with the PIP_2-bound 3SPI crystal structure, we also performed atomistic simulations of this PIP_2-bound structure. These reference simulations provide a more valid comparison with the multiscale simulations, because it is then possible to directly compare simulations of both proteins embedded in a phospholipid bilayer at room temperature, rather than comparing a membrane-bound simulation with a static X-ray structure in the absence of a membrane.

Examination of the 3SPI crystal structure shows that residues that make contacts with the PIP_2 headgroup (Figure 1A) are mostly basic and are located on either the N-terminal end of the first transmembrane helix TM1 (R78, W79, and R80) or the C-linker that connects the TMD with the CTD (K183, R186, K188, and K189).[14] We found that in the reference simulation of this structure all PIP_2−protein contacts were retained and accounted for nearly 90% of the total contacts made by side chains with the PIP_2 headgroups (Figure 1B). Those residues that made less frequent contacts (∼5%) with the PIP_2 headgroups (K183 and R186) were located on the C-linker. The C-linker is helical in the PIP_2-bound 3SPI structure, but flexible in other Kir2.2 crystal structures, and may therefore account for the differences observed for K183 and R186 in these simulations. However, the reference simulations appear to confirm the stability of the 3SPI structure and of the PIP_2−protein interactions in this structure.
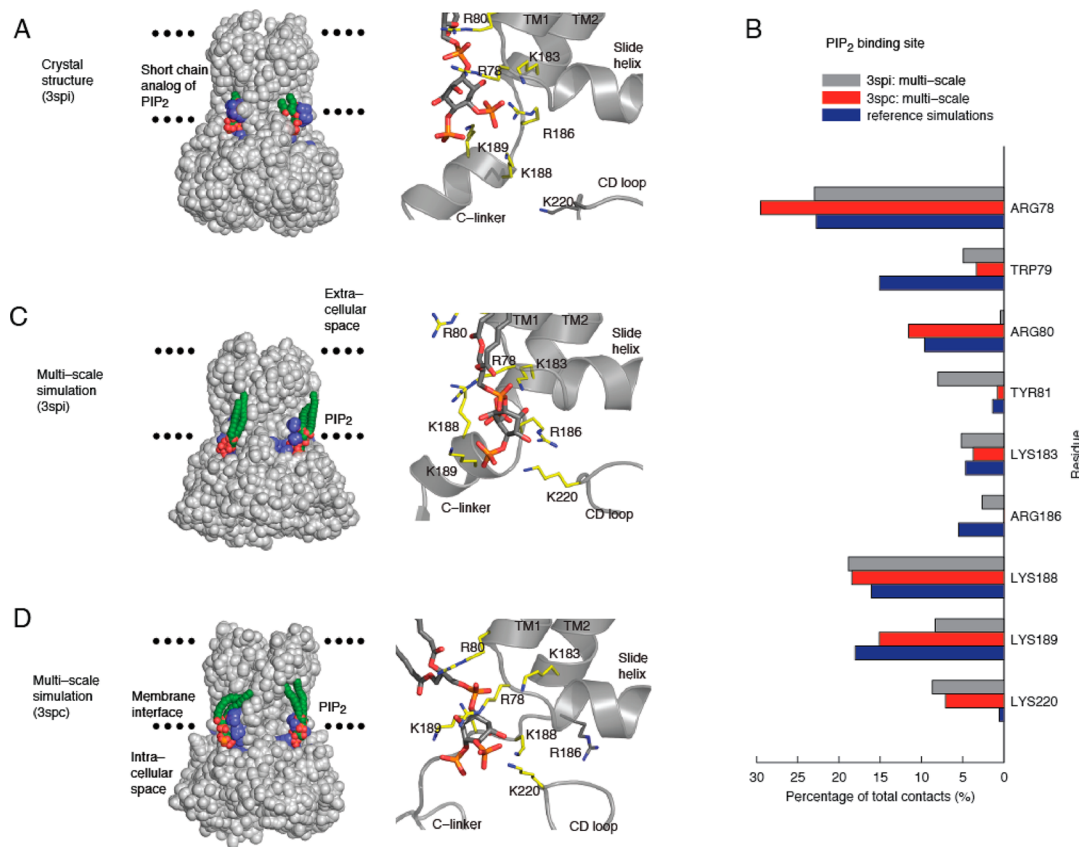
Figure 1. PIP$_2$ binding in Kir2.2 multiscale simulations. (A) Crystal structure with PIP$_2$ bound. For clarity, only two PIP$_2$ molecules are shown, with PIP$_2$-interacting residues colored blue (left). Detailed view of the PIP$_2$ binding site (right) as found in the 3SPI structure. (B) Multiscale simulations used either 3SPI or 3SPC as the starting structure and combined coarse-grained (CG; 24 × 0.5 μs) and atomistic (AT; 2 × 0.1 μs) simulations. Reference simulations were AT (2 × 0.1 μs) of the PIP$_2$-bound 3SPI crystal structure. Residues whose side chains make more than 5% of the total contacts (≤4 Å) with PIP$_2$ headgroups are compared between the multiscale and reference simulations. (C and D) Binding site of PIP$_2$ predicted by a (C) 3SPI or (D) 3SPC multiscale simulation. Parameters for PIP$_2$ can be found in the Supporting Information (Figure S4 and Table 1).

Importantly, we found that the multiscale simulations that used the protein coordinates from 3SPI as a starting structure predicted the PIP$_2$ headgroup to bind to the same cluster of basic residues as observed in the crystal structure (Figure 1C). This is in excellent agreement with both the reference simulations of this structure and earlier predictions for other Kir channels.[5,6] Residues on TM1 (R78) and on the C-linker (K183, R186, K188, and K189) were found to form the same number of contacts in the 3SPI multiscale simulations as in the reference simulations (Figure 1B). Residue W79 on TM1 formed fewer contacts in the multiscale simulations (5%) than in the reference simulations (15%). The absence of any specific hydrogen bond interactions of W79 with PIP$_2$ in the crystal structure is likely to render the orientation of this side chain more flexible and might be the reason for less frequent contacts between W79 and PIP$_2$ in the multiscale simulations compared to the reference simulations. Although W79 is suggested to facilitate PIP$_2$ binding by anchoring TM1 at the membrane interface,[14] less frequent contacts argue against a direct interaction of W79 with PIP$_2$. The two adjacent residues (R80 and Y81) also exhibit differences between the multiscale and reference simulations, but this is most likely to be related to changes in TM2 that occur during the onset of channel gating. Nevertheless, these results demonstrate agreement among the PIP$_2$-bound 3SPI crystal structure, the 3SPI multiscale simulations, and the reference simulations.

In addition to using 3SPI, we also used the 3SPC protein coordinates as an input for the multiscale predictions. This structure was crystallized with the anionic phospholipid PPA instead of PIP$_2$ and more closely resembles the apo-state structure (3JYC) in which the CTD is detached and not fully engaged with the TMD.[14] Strikingly, we found that when the ligand-free 3SPC structure was used as a starting point for the multiscale simulations of PIP$_2$ binding, there was also good agreement between the multiscale simulations and reference simulations (Figure 1D). Almost all contacts that were observed in the reference simulations were predicted by the 3SPC multiscale simulations (Figure 1B) and were similar to those using 3SPI as a starting structure. The only major difference was the absence of any interaction between the headgroup of PIP$_2$ and R186 (Figure 1B). This is probably because in the 3SPC starting structure this "C-linker" is less well ordered and the R186 side chain points in the opposite direction when compared to the PIP$_2$-bound 3SPI structure. Longer simulations may therefore be needed to see if R186 changes its orientation to interact with the PIP$_2$ headgroup.

Together, these results clearly demonstrate that the multi-scale simulation approach can accurately predict the binding site for PIP$_2$ in Kir2.2 even when slightly different input structures are used. The principal advantage of the multiscale approach compared to conventional docking methods is that both PIP$_2$ and the Kir2.2 channel are flexible. This can therefore provide insights into the molecular mechanisms

underlying PIP$_2$ binding, such as conformational changes or an electrostatic contribution (Figure S2 of the Supporting Information), which more static docking approaches lack. Interestingly, during the simulations, we observed that the phosphates of the PIP$_2$ headgroup formed transient hydrogen bonds with K220 on the CD loop. This resulted in a decrease in the C$_\alpha$−C$_\alpha$ distance between K220 and a highly conserved aspartate on the slide helix (D76) of 2−4 Å. This motion appears to be due to the CD loop moving upward toward the slide helix and C-linker during PIP$_2$ binding, similar to the gating mechanism proposed in several other studies[16,17] and which may form part of a general activation mechanism for Kir channels by PIP$_2$.[6] Our results also suggest that binding of PIP$_2$ to the C-linker stabilizes its α-helical structure and may account for the interaction of PIP$_2$ with R186 in the 3SPI crystal structure. Moreover, using the multiscale approach, the effect of lipid bilayer composition on PIP$_2$ binding can be studied. Studies of liposomes with a controlled lipid composition highlighted an anionic secondary lipid requirement for PIP$_2$-induced Kir channel activation.[18] We therefore repeated our CG simulations, replacing half of the lipids on the inner leaflet with the anionic phospholipid phosphatidylserine (PS), noting that PIP$_2$ still binds to Kir2.2, while PS, accumulating on either side of the slide helix, is distributed unevenly around Kir2.2 (Figure S3 of the Supporting Information). This suggests a secondary binding site for anionic lipids in Kir channels.

In conclusion, these findings demonstrate good agreement among the PIP$_2$-bound crystal structure, the multiscale predictions, and the reference simulations and therefore validate this multiscale approach[5,6] for the prediction of PIP$_2$ binding sites. Consequently, this method may be confidently applied to the prediction of novel PIP$_2$ binding sites as well as the exploration of other lipid−channel interactions. For example, several eukaryotic voltage-gated potassium channels are regulated by PIP$_2$,[19,20] and enough high-resolution crystal structures now exist to allow similar multiscale simulations of binding of PIP$_2$ to these structures. Also, cholesterol has been shown to directly regulate Kir channel function, but its precise binding site is unknown.[21] Many other unrelated ion channels and transporters, as well other classes of membrane proteins, have also been shown to be regulated by lipids.[22−24] Therefore, this multiscale approach now provides an important and powerful tool for helping to study protein−lipid interactions and will become increasingly important with the ever-expanding number of high-resolution membrane protein crystal structures now available.

■ ASSOCIATED CONTENT

Ⓢ Supporting Information

Detailed methods, PIP$_2$ binding to an apo structure (PDB entry 3JYC), electrostatic potential mapped on the PIP$_2$ binding site, simulations in a mixed bilayer, and the root-mean-square fluctuations of the PIP$_2$ binding site. This material is available free of charge via the Internet at http://pubs.acs.org.

■ AUTHOR INFORMATION

Corresponding Author

*Phone: +44 1865 613306. E-mail: mark.sansom@bioch.ox.ac.uk.

Notes

The authors declare no competing financial interests.

■ ACKNOWLEDGMENTS

■ REFERENCES

(1) Suh, B. C., and Hille, B. (2008) *Annu. Rev. Biophys. 37*, 175−195.
(2) Ashcroft, F. M. (2006) *Nature 440*, 440−447.
(3) Lopes, C. M., Zhang, H., Rohacs, T., Jin, T., Yang, J., and Logothetis, D. E. (2002) *Neuron 34*, 933−944.
(4) Haider, S., Tarasov, A. I., Craig, T. J., Sansom, M. S., and Ashcroft, F. M. (2007) *EMBO J. 26*, 3749−3759.
(5) Stansfeld, P. J., Hopkinson, R., Ashcroft, F. M., and Sansom, M. S. (2009) *Biochemistry 48*, 10926−10933.
(6) Meng, X.-Y., Zhang, H.-X., Logothetis, D. E., and Cui, M. (2012) *Biophys. J. 102*, 2049−2059.
(7) Leal-Pinto, E., Gómez-Llorente, Y., Sundaram, S., Tang, Q.-Y., Ivanova-Nikolova, T., Mahajan, R., Baki, L., Zhang, Z., Chavez, J., Ubarretxena-Belandia, I., and Logothetis, D. E. (2010) *J. Biol. Chem. 285*, 39790−39800.
(8) D'Avanzo, N., Cheng, W. W. L., Doyle, D. A., and Nichols, C. G. (2010) *J. Biol. Chem. 285*, 37129−37132.
(9) Stansfeld, P. J., and Sansom, M. S. P. (2011) *J. Chem. Theory Comput. 7*, 1157−1166.
(10) Monticelli, L., Kandasamy, S. K., Periole, X., Larson, R. G., Tieleman, D. P., and Marrink, S.-J. (2008) *J. Chem. Theory Comput. 4*, 819−834.
(11) Berger, O., Edholm, O., and Jähnig, F. (1997) *Biophys. J. 72*, 2002−2013.
(12) Scott, W. R. P., Hunenberger, P. H., Tironi, I. G., Mark, A. E., Billeter, S. R., Fennen, J., Torda, A. E., Huber, T., Kruger, P., and Van Gunsteren, W. F. (1999) *J. Phys. Chem. A 103*, 3596−3607.
(13) Hess, B., Kutzner, C., Van der Spoel, D., and Lindahl, E. (2008) *J. Chem. Theory Comput. 4*, 435−447.
(14) Hansen, S. B., Tao, X., and MacKinnon, R. (2011) *Nature 477*, 495−498.
(15) Tao, X., Avalos, J. L., Chen, J., and MacKinnon, R. (2009) *Science 326*, 1668−1674.
(16) Whorton, M. R., and MacKinnon, R. (2011) *Cell 147*, 199−208.
(17) Bavro, V. N., De Zorzi, R., Schmidt, M. R., Muniz, J. R. C., Zubcevic, L., Sansom, M. S. P., Vénien-Bryan, C., and Tucker, S. J. (2012) *Nat. Struct. Mol. Biol. 19*, 158−163.
(18) Cheng, W. W. L., D'Avanzo, N., Doyle, D. A., and Nichols, C. G. (2011) *Biophys. J. 100*, 620−628.
(19) Rodriguez-Menchaca, A. A., Adney, S. K., Tang, Q.-Y., Meng, X.-Y., Rosenhouse-Dantsker, A., Cui, M., and Logothetis, D. E. (2012) *Proc. Natl. Acad. Sci. U.S.A. 109*, 2399−2408.
(20) Kruse, M., Hammond, G. R. V., and Hille, B. (2012) *J. Gen. Physiol. 140*, 189−205.
(21) Rosenhouse-Dantsker, A., Logothetis, D. E., and Levitan, I. (2011) *Biophys. J. 100*, 381−389.
(22) Tucker, S. J., and Baukrowitz, T. (2008) *J. Gen. Physiol. 131*, 431−438.
(23) Coskun, U., and Simons, K. (2011) *Structure 19*, 1543−1548.
(24) Aponte-Santamaría, C., Briones, R., Schenk, A. D., Walz, T., and De Groot, B. L. (2012) *Proc. Natl. Acad. Sci. U.S.A. 109*, 9887−9892.

SUPPORTING INFORMATION

The main article predicts the binding site of phosphatidylinositol 4,5-bisphosphate (PIP$_2$) on the inwardly-rectifying potassium channel Kir2.2 and reports good agreement between our prediction and the binding site of PIP$_2$ observed in a crystal structure of Kir2.2 (PDB id 3SPI). In this supporting information, we provide detailed methods describing the setup and the analysis of the coarse-grained (CG) and atomistic (AT) molecular dynamics simulations (Figures S1 and S3), the electrostatic potential mapped on the binding site of PIP$_2$ (Figure S2), and the CG force field parameters used for PIP$_2$ (Figure S4 and Table 1).

Supplementary methods

The PIP$_2$ binding site was predicted using a multi-scale approach, consisting of CG simulations, which were then followed by AT simulations. Two crystal structures of Kir2.2, wt-Kir2.2 bound to a short-chain (scPIP$_2$) derivative of PIP$_2$ (PDB id 3SPI), and wt-Kir2.2 bound to an anionic lipid (PDB id 3SPC), were used as starting structures of the multi-scale simulations. In order to prepare the starting structures of the multi-scale simulations, we removed scPIP$_2$ and the anionic lipid, and embedded the structures into a 1-palmitoyl, 2-oleoyl-sn-glycero-3-phosphocholine (POPC) lipid bilayer, with four PIP$_2$ molecules added to the in the intracellular leaflet (Figure S1A). Unresolved residues in the N-terminus of the 3SPC structure were modeled after 3SPI. For each starting structure, CG simulations (24 x 0.5 µs) were performed using the Martini parameters, showing binding of PIP$_2$ to the protein (Figure S1B). Snapshots were taken at 0.5 µs from CG simulations, and converted into atomistic systems. The coarse-grained protein was converted into an atomistic representation using the 'align' option (1), by realignment of the original atomistic PDB coordinates that were used as starting structures of the multi-scale simulations. Gromos96 43a1, Berger lipid parameters, and the SPC water model were used for AT simulations (2 x 100 ns / starting structure). We prepared the systems for AT simulations by placing potassium ions at position S2 and S4 of the selectivity filter and solvated the cavity below the selectivity filter using Voidoo (2). Before the start of the AT simulations, systems were energy-minimized using 5000 iterations of steepest descent, followed by a 1 ns AT simulation with positional restraints of 1000 kJ/mol/nm^2 applied in each direction to the protein's heavy atoms. In addition to 3SPC and 3SPI multi-scale simulations, CG simulations of the apo structure of wt-Kir2.2 (PDB id 3JYC), although not converted into AT, suggest that PIP$_2$ may be able to bind to Kir2.2 in the apo-state as well (Figure S1C).

As noted in the main text, basic residues predicted to bind PIP$_2$ coincide with regions of positive electrostatic potential on Kir2.2 (Figure S2). To test for a possible influence of the lipid bilayer composition on PIP$_2$ binding, CG simulations were repeated with half of the inner leaflet POPC lipids randomly replaced by the anionic lipid 1-palmitoyl, 2-oleoyl-sn-glycero-3-phosphatidylserine (POPS) (Figure S3).

The reference simulations (2 x 100 ns) were performed with PIP$_2$ placed in the location in which scPIP$_2$ was observed in the crystal structure (PDB id 3SPI). In order to set up the reference simulations, we performed a 0.1 µs CG self-assembly simulation of 3SPI in POPC, followed by conversion into an atomistic system (using the 'align' option). We aligned the head groups of PIP$_2$ and scPIP$_2$ and removed any clashing lipids. After energy minimization of the system, we applied positional restraints of 1000 kJ/mol/nm^2 in each direction for 1 ns to the protein's heavy atoms and to the head group atoms C$_1$-C$_6$ of PIP$_2$ followed by 100 ns of unrestrained AT simulation. This ensured that, at the start of the unrestrained 100 ns reference simulations, the coordinates for PIP$_2$ coincided with the coordinates of scPIP$_2$ from the crystal structure. The reference simulations were repeated with PIP$_2$ removed from the protein before the start of the simulation ("equilibration", 2 x 100 ns, Figure S5), to test whether the lipid-bound structure was able to equilibrate into a structure similar to the Kir2.2 apo-state, and RMSF values computed using Gromacs4.5.5 (Figure S5).

Figure S1

S1A
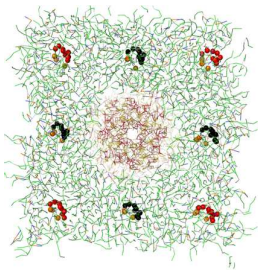
S1C
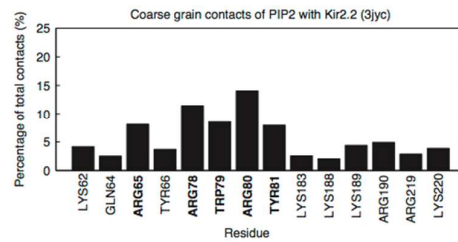
S1B
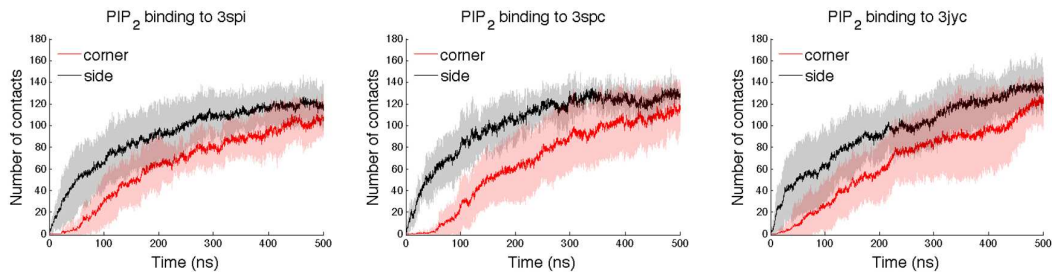
Figure S1A. Setup of a coarse-grained (CG) binding simulation. Before the start of the simulation (t=0 μs), PIP$_2$ is added to the lower leaflet of the lipid bilayer, in two different starting locations: either to the corners of the simulation box (red CG PIP$_2$ particles), or to the sides of the simulation box (black CG PIP$_2$ particles).

Figure S1B. Average number of contacts between the PIP$_2$ head groups and Kir2.2 in CG simulations for each starting configuration, and each input structure (PDB ids 3SPI, 3SPC and 3JYC).

Figure S1C. Residues making contacts with PIP$_2$ head groups in coarse-grained simulations of the apo state (PDB id 3JYC, residues in bold account for >5% of the total contacts).

Figure S2
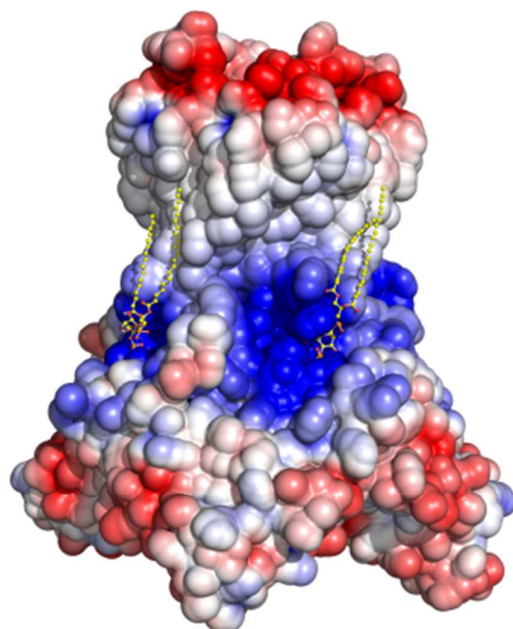
Figure S2. Snapshot from a 3spi multi–scale prediction, after 100 ns of atomistic simulation, colored by electrostatic potential. PDB2PQR (3) and PROPKA (4) were used to assign charges, radii, and protonation states. APBS Tools (5) and Pymol (6) were used to map the electrostatic potential, colored from -4 kT/e (red) to $+4$ kT/e (blue), onto the solvent-accessible surface. PIP_2 is shown in a ball and stick representation. The binding site of the PIP_2 head group coincides with areas of positive electrostatic potential.

Figure S3

S3A

S3B

PIP$_2$ POPS

Figure S3A. Comparison between the average number of contacts between PIP$_2$ head groups and Kir2.2 (PDB id 3SPC) in coarse-grained (CG) simulations, for a neutral POPC bilayer (black), and for a bilayer in which half of the inner leaflet POPC molecules were replaced by the anionic lipid POPS (red).

Figure S3B. Average distribution of PIP$_2$ (left) and POPS (right) around Kir2.2 (PDB id 3SPI) during a CG simulation, as seen from the extracellular side, with half of the inner leaflet POPC molecules replaced by POPS. Color indicates low (blue) or high density (red) of normalized lipid distribution. Three of four PIP$_2$ molecules are bound in this CG simulation. VMD and Bendix were used for visualization(7, 8).

Figure S4

PIP$_2$ POPS   POPC

Figure S4. Martini particle types used for coarse-grained (CG) simulations (also see Table 1). The Martini 2.1 force field (9-11) parameters were used for POPS and POPC lipids.

Table 1. Coarse-grained force field parameters for PIP$_2$.

```
[moleculetype]
; molname       nrexcl
  PIP2  1
[atoms]
; id    type    resnr   residu  atom    cgnr    charge
  1     Qa      1       PIP2    PO1     1       -2.0
  2     Qa      1       PIP2    PO2     2       -2.0
  3     SP1     1       PIP2    RP1     3       0
  4     SP1     1       PIP2    RP2     4       0
  5     SP1     1       PIP2    RP3     5       0
  6     Qa      1       PIP2    PO3     6       -1.0
  7     Na      1       PIP2    GL1     7       0
  8     Na      1       PIP2    GL2     8       0
  9     C1      1       PIP2    C1A     9       0
  10    C1      1       PIP2    C2A     10      0
  11    C1      1       PIP2    C3A     11      0
  12    C1      1       PIP2    C4A     12      0
  13    C1      1       PIP2    C1B     13      0
  14    C1      1       PIP2    C2B     14      0
  15    C1      1       PIP2    C3B     15      0
  16    C1      1       PIP2    C4B     16      0
  17    C1      1       PIP2    C5B     17      0
[bonds]
; i j  funct   length  force.c.
  1 3  1       0.30    5000
  2 3  1       0.34    5000
  2 4  1       0.34    5000
  3 4  1       0.30    20000
  3 5  1       0.30    20000
  4 5  1       0.30    20000
  5 6  1       0.30    5000
  6 7  1       0.47    1250
  7 8  1       0.37    1250
  8 9  1       0.47    1250
  9 10 1       0.47    1250
  10 11 1      0.47    1250
  11 12 1      0.47    1250
  7  13 1      0.47    1250
  13 14 1      0.47    1250
  14 15 1      0.47    1250
  15 16 1      0.47    1250
  16 17 1      0.47    1250
[angles]
; i j k         funct   angle   force.c.
  1 3 6         2       180.0   45.0
  2 4 6         2       120.0   45.0
  1 5 6         2       180.0   45.0
  2 5 6         2       180.0   45.0
  3 4 5         2       120.0   25.0
  4 5 3         2       120.0   25.0
  5 6 7         2       180.0   25.0
  6 7 8         2       120.0   25.0
  6 7 13        2       180.0   25.0
  7 8 9         2       180.0   25.0
  8 9 10        2       180.0   25.0
  9 10 11       2       180.0   25.0
  10 11 12      2       180.0   25.0
  7 13 14       2       180.0   25.0
  13 14 15      2       180.0   25.0
  14 15 16      2       180.0   25.0
  15 16 17      2       180.0   25.0
```

Figure S5

S5A
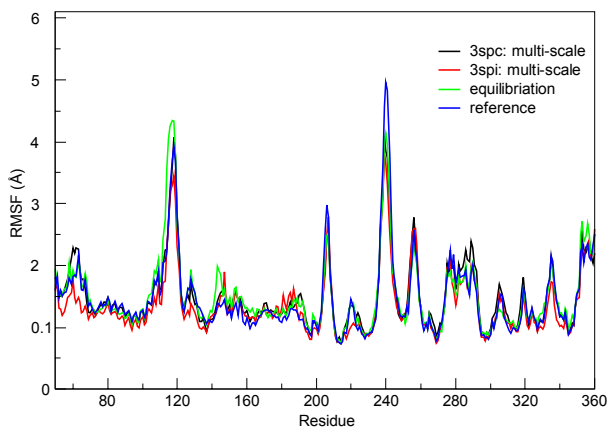
S5B
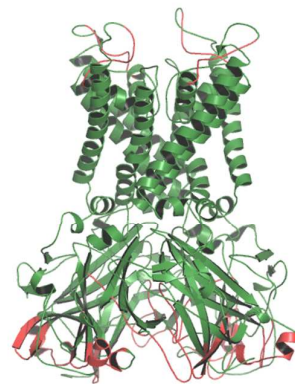
S5C
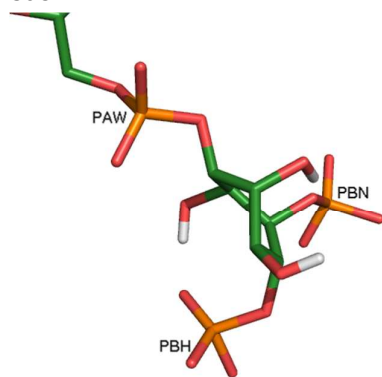
S5D
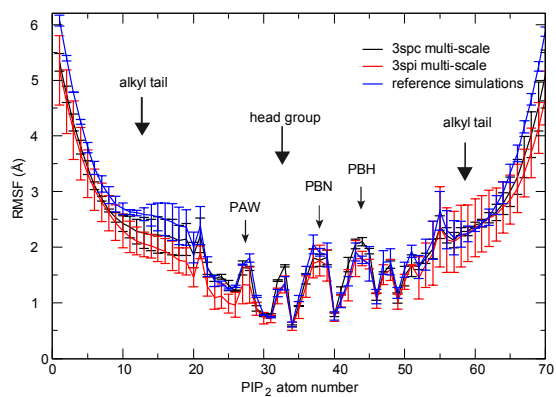
Figure S5A. Average root mean square fluctuations (RMSF) of C_α atoms, calculated for 3spc and 3spi multi-scale simulations (2 x 100 ns / input structure), reference simulations (2 x 100 ns), and equilibration simulations (3spi, PIP_2 removed, 2 x 100 ns).

Figure S5B. Residues with average RMSF > 2.5 Å (red) mapped on a snapshot of an atomistic simulation.

Figure S5C. Nomenclature used in Figure S5C.

Figure S5D. Average RMSF of PIP_2. Phosphates (PAW, PBN and PBH) with adjacent oxygen atoms are highlighted by small arrows.

Supplementary references:

1.   Stansfeld, P. J., and Sansom, M. S. P. (2011) From coarse grained to atomistic: a serial multiscale approach to membrane protein simulations., *J. Chem. Theory Comput*. 7, 1157–1166.

2.   Kleywegt, G. J., and Jones, T. A. (1994) Detection, delineation, measurement and display of cavities in macromolecular structures, *Acta Crystallogr. D*. 50, 178–185.

3.   Dolinsky, T. J., Czodrowski, P., Li, H., Nielsen, J. E., Jensen, J. H., Klebe, G., and Baker, N. A. (2007) Pdb2pqr: expanding and upgrading automated preparation of biomolecular structures for molecular simulations., *Nucleic Acids Res*. 35, W522–5.

4.   Li, H., Robertson, A. D., and Jensen, J. H. (2005) Very fast empirical prediction and rationalization of protein pKa values., *Proteins*. 61, 704–721.

5.   Holst, M. J., and Saied, F. (1995) Numerical solution of the nonlinear Poisson-Boltzmann equation: developing more robust and efficient methods, *J. Comp. Chem*. 16, 337–364.

6.   DeLano, W. L. (2002) The PyMOL molecular graphics system.

7.   Humphrey, W., Dalke A., Schulten K. (1996) VMD: visual molecular dynamics, *Journal of Molecular Graphics*. 14, 33–38.

8.   Dahl, A. C. E., Chavent, M., and Sansom, M. S. P. (2012) Bendix: intuitive helix geometry analysis and abstraction., *Bioinformatics*. 28, 2193–2194.

9.   Marrink, S. J., De Vries, A. H., and Mark, A. E. (2004) Coarse grained model for semiquantitative lipid simulations, *J. Phys. Chem. B*. 108, 750–760.

10.   Monticelli, L., Kandasamy, S. K., Periole, X., Larson, R. G., Tieleman, D. P., and Marrink, S.-J. (2008) The Martini coarse-grained force field: extension to proteins., *J. Chem. Theory Comput*. 4, 819–834.

11   Marrink, S. J., Risselada, H. J., Yefimov, S., Tieleman, D. P., and De Vries, A. H. (2007) The Martini force field: coarse grained model for biomolecular simulations., *J. Phys. Chem. B*. 111, 7812–7824.